Generation of optical vortices by using binary vortex producing lenses

N. Londoño,[1] E. Rueda,[1,*] J. A. Gómez,[2] and A. Lencina[3,4]

[1]Grupo de Óptica y Fotónica, Instituto de Física, Universidad de Antioquia U de A, Calle 70 No. 52-21, Medellín, Colombia

[2]Grupo de Física Básica y Aplicada, Politécnico Colombiano Jaime Isaza Cadavid, Medellín, Colombia

[3]Centro de Investigaciones Ópticas (CONICET La Plata-CIC), P.O. Box 3, (1897) Gonnet, Argentina

[4]Departamento de Física, Facultad de Ciencias Exactas Universidad Nacional de La Plata, La Plata, Argentina

*Corresponding author: edgar.rueda@udea.edu.co

Received 26 September 2014; revised 3 December 2014; accepted 22 December 2014; posted 22 December 2014 (Doc. ID 223906); published 26 January 2015

Experimental high-quality optical vortices of different topological charges are generated by using a vortex producing lens with two phase levels. In our setup, the lens is displayed on a liquid-crystal spatial light modulator that only attains phase modulation of around 1.2π. This achievement opens the real possibility of creating high-quality optical vortices with devices of very low phase modulation capacity. The experimental setup is fully described, and the considerations to set the optimal parameters to obtain high-quality optical vortices are discussed and experimentally established. The phase and intensity of the optical vortices are recovered. The phase is obtained through a phase-shifting method that is directly programmed onto the modulator avoiding any class of mechanical displacement.

OCIS codes: (050.4865) Optical vortices; (070.6120) Spatial light modulators; (050.1940) Diffraction.
http://dx.doi.org/10.1364/AO.54.000796

1. Introduction

One property shared by all waves is the possibility to have phase singularities [1]. In the case of electromagnetic waves, these singularities are commonly known as optical vortices (OVs). OVs are localizations in space, points for 2D and lines for 3D, where the amplitude of the wave is zero and the phase is undefined [2,3], while its surroundings are characterized by the presence of a helicoidal wave defined by the phase term $\exp(im\theta)$, where θ is the azimuthal angle and m is the vortex topological charge, which represents the number of 2π discontinuities of the wavefront [4]. The Poynting vector of these beams has an azimuthal component around the vortex; thus they have a well-defined optical angular momentum (OAM) parallel to the optical axis [5,6]. Due to these and other features, OVs have been widely used in applications for optical pattern formation systems [7], optical tweezers [8–10], metrology [11,12], image processing [13,14], quantum data encryption [15,16], and stellar choronography [17], among others.

Laguerre–Gauss (L-G) functions are the most widely used mathematical representations for OVs in science and engineering, thanks to their donut-shaped intensity pattern form and to their phase linear azimuthal dependency around the symmetry axis [18]. To experimentally generate this kind of beam a Gaussian beam is directed toward a phase mask programmed onto a liquid-crystal spatial light modulator (LC-SLM). For a phase mask it is possible to use a spiral phase plate (SPP) defined by the equation $t(\theta) = \exp(im\theta)$ [19], or a vortex producing lens (VPL) defined by the equation $t(r,\theta) = e^{im\theta}e^{-i\frac{\pi r^2}{\lambda f_{\mathrm{FR}}}}$, which corresponds to the product of a SPP with a Fresnel lens of focal distance f_{FR} and wavelength λ

1559-128X/15/040796-06$15.00/0

[20]. When displaying a phase mask on a LC-SLM it is necessary to discretize the phase into N levels depending on the characteristics of the LC-SLM. For the ideal case, with an 8 bit dynamic range, 256 phase levels can be addressed by the modulator. But, in the case of transmission LC-SLMs, it is common that in the search for a uniform amplitude response the phase modulation is reduced, thus achieving a phase modulation lower than 2π rad. To overcome this difficulty, the phase mask is discretized into a number of levels depending on the maximum obtained phase modulation ($\theta_{\max}$), $N \leq 2\pi/(2\pi - \theta_{\max})$ [20]. In this sense, Gou *et al.* [21] and Kotlyar and Kovalev [22] showed that the OV intensity pattern depends directly on the number of phase levels used to discretize the phase of a SPP. Additionally, Zhang *et al.* [23] experimentally showed that to generate a good quality OV it is necessary to program $N \geq 6$ phase levels. These results imply that to generate in the laboratory an OV by means of a SPP it is necessary to use a LC-SLM with a phase modulation of at least $5\pi/3$. Nevertheless, recently Rueda *et al.* [20] showed that it is possible to generate a high-quality OV with a few numbers of levels, if one uses a multilevel phase plate VPL. They generated experimentally high-quality OVs by using a four-level VPL, corresponding to a maximum modulation of $\theta_{\max} \approx 3\pi/2$.

In this work, we experimentally obtain high-quality OVs, with charges between $m = 1$ and $m = 5$, by using a two-level VPL. This binary vortex producing lens (BVPL) is displayed in a low-capacity LC-SLM with a maximum phase modulation of $\theta_{\max} \approx 1.2\pi$. To analyze the quality of the OVs their intensity and phase are measured with a CMOS camera and a phase-shifting interferometry (PSI) technique with its steps directly programmed on the LC-SLM [24], respectively. The obtained experimental results are then compared with the simulated ideal case of a 256-level SPP. The results showed with no doubt that by using BVPLs, high-quality OVs can be generated with the minimum possible number of levels. Additionally, the most relevant parameters of the experimental optical setup are analyzed in order to achieve the maximum quality of the OV.

2. Experimental Analysis and Results

The main consideration to implement discrete phase masks on spatial light modulators is the knowledge of their phase and amplitude responses. In our case, the experimental setup was developed by using a LC-SLM Holoeye LC2002, whose phase calibration for $\lambda = 532$ nm is presented in Fig. 1. Here, it is important to highlight that the experimental phase and amplitude characteristics obtained for the Holoeye LC2002 illustrate the typical behavior of a wide group of low-cost LC-SLMs, commonly used in scientific and technological applications. Analyzing the calibration curves, it is evident that the amplitude response is very uniform (variations lower than 10%), guaranteeing a good approximation to pure phase modulation. However, with this operating condition the maximum phase modulation is under 2π, and, therefore, the phase masks displayed on the LC-SLM must be discretized.

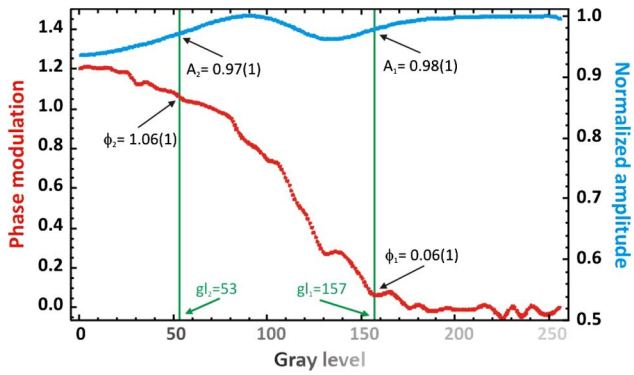

Fig. 1. Phase and amplitude response of the LC-SLM Holoeye LC2002 at $\lambda = 532$ nm.

In particular, the operating characteristics of our LC-SLM showed that the maximum phase modulation is $\theta_{\max} = 1.2\pi$, which is equivalent to address $N = 2$ phase levels. Thus, to experimentally build a discrete mask, two gray levels with identical amplitude response and phase difference of π must be chosen. In our case, these conditions were satisfied for the phase values $\varphi = 1.06\pi$ and $\varphi = 0.06\pi$, which correspond to gray levels 53 and 157, respectively (see Fig. 1).

After the selection of the phase levels, the corresponding transmittance BVPL function was built. To create this type of phase mask, it is necessary to consider some parameters that guarantee that the minimum focal length of the implemented Fresnel lens is sampled adequately. These parameters are the illumination wavelength, the pixel size pix, and the width a of the LC-SLM window. In our case, the laser source was an Nd:Yag emitting at $\lambda = 532$ nm, and the LC-SLM was a Holoeye LC2002 with pixel size of pix $= 32$ μm and a window of 800×600 pixels. Based on these experimental parameters, the minimum f_{FR} modulus is defined as $|f_{\mathrm{FR}}| = \frac{800(\mathrm{pix})^2}{\lambda}$. In Fig. 2, the sequence for the construction of a BVPL with $m = 1$ is presented. Initially, a SPP and a convergent Fresnel lens are generated and superposed forming a VPL of 256 levels, and then the obtained VPL is discretized according to the possible phase levels—in this case two-phase levels.

To generate and characterize the OVs, the BVPL is displayed in the LC-SLM of the experimental setup presented in Fig. 3. There, linear polarizers P_1, P_2 and the $\lambda/4$ waveplate are introduced to guarantee the desired phase and amplitude responses shown in Fig. 1. The laser beam is spatially filtered and collimated with the spatial filter O and lens L_1, respectively, and the beam diameter $2w$ is adjusted with diaphragm D. Subsequently, the beam passes through a Mach–Zehnder interferometer formed by beam splitters BS_1, BS_2 and mirrors M_1 and M_2. One arm of the interferometer is used as a reference wave for the phase retrieval (the linear polarizer P_3 allows

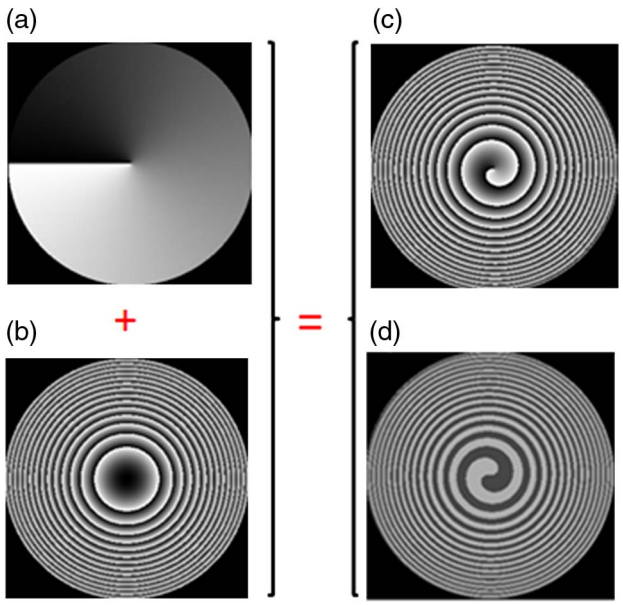

Fig. 2. Construction of BVPL for $m = 1$. (a) SPP with $N = 256$, (b) convergent Fresnel lens with $N = 256$ (2π modulation), (c) superposition of the SPP and the Fresnel lens to create a VPL with $N = 256$, and (d) two-phase levels discretized VPL (BVPL).

controlling the intensity of the beam), while on the other arm the LC-SLM displays the BVPL that generates the OVs. Light emerging from the LC-SLM is focalized with a convergent lens L_2 located at a distance f (equal to its focal length of 250 mm) of the LC-SLM. The OV is observed at a distance z_{opt} measured from the focal plane of L_2, where $z_{\text{opt}} = f^2/f_{\text{FR}}$ [20,25]. To obtain the amplitude of the OV at the observation plane an optical shutter (OS) in the reference arm is closed and the intensity is registered by using a CMOS camera coupled to a 20× microscope objective. To obtain the phase map the OS is open and a five-step PSI algorithm is implemented by encoding the phase delays directly in the LC-SLM [24].

In Fig. 4, results for topological charges $m = 1$ to $m = 5$ are shown. There, the OVs generated by using simulated two-phase level and 256-phase level SPPs were compared with the experimental results of the implementation of a two-phase level SPP and BVPL. Additionally, the results of simulating the OVs with BVPLs are depicted. It is important to emphasize that in the case of the OV generated by SPPs, no Fresnel lens is displayed in the LC-SLM; therefore, the observation plane coincides with the focal plane of lens L_2, whereas for the OV generated by the BVPL, the corresponding observation plane is located at a distance $z_{\text{opt}} \approx 40.6$ mm, measured from the focal plane of the lens, when $f_{\text{FR}} = -1.54$ m.

Comparisons of the simulated and experimental results indicate that the experimental OVs obtained by using two-phase level SPPs were in agreement with the OVs calculated computationally, which do not correspond to a beam of the L-G type; i.e., the intensity pattern in the observation plane did not correspond to the donut-shaped pattern expected for a L-G-like OV. Now, results obtained by the BVPLs, unlike the previous case, present an intensity pattern very similar to the L-G OV type. Likewise, the phase distribution of the OVs generated by the BVPLs has the same quality of simulated optical vortices of 256 levels. Minor experimental phase distortions can be attributed to the optical aberrations of the experimental system [26].

The previous experimental results prove that it is possible to obtain high-quality optical vortices by using BVPLs. Nevertheless, we show below that some parameters of the system can affect the quality of the technique if they are not properly chosen.

3. Experimental Optimization

When the OVs are generated by using VPLs there are two additional parameters that must be considered and that do not appear when SPPs are used; they are the focal length of the Fresnel lens and the appropriated observation plane. The value of these parameters significantly influences the quality of the OV, and, therefore, if they are not chosen adequately they can affect the intensity and phase distributions of the vortices, distorting them with respect to the ideal form (L-G-type distribution). To quantitatively evaluate the quality of the vortex when these parameters were changed, a modified mean square error (MSE), defined in Eq. (1), was calculated. The MSE was computed between OVs

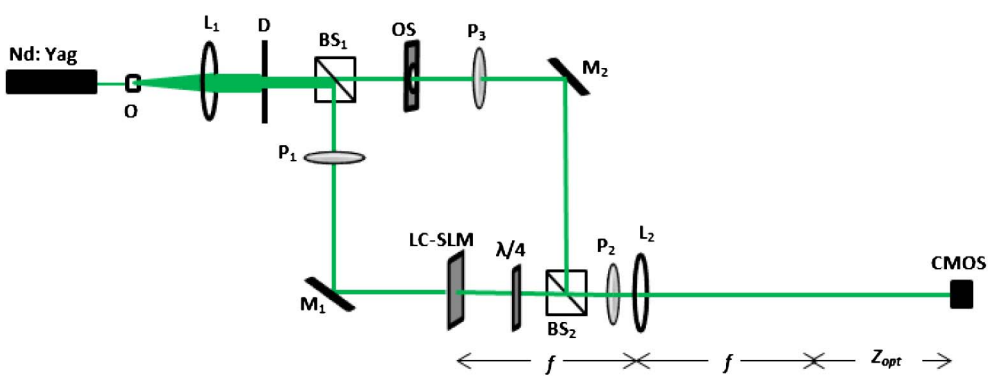

Fig. 3. Experimental setup.

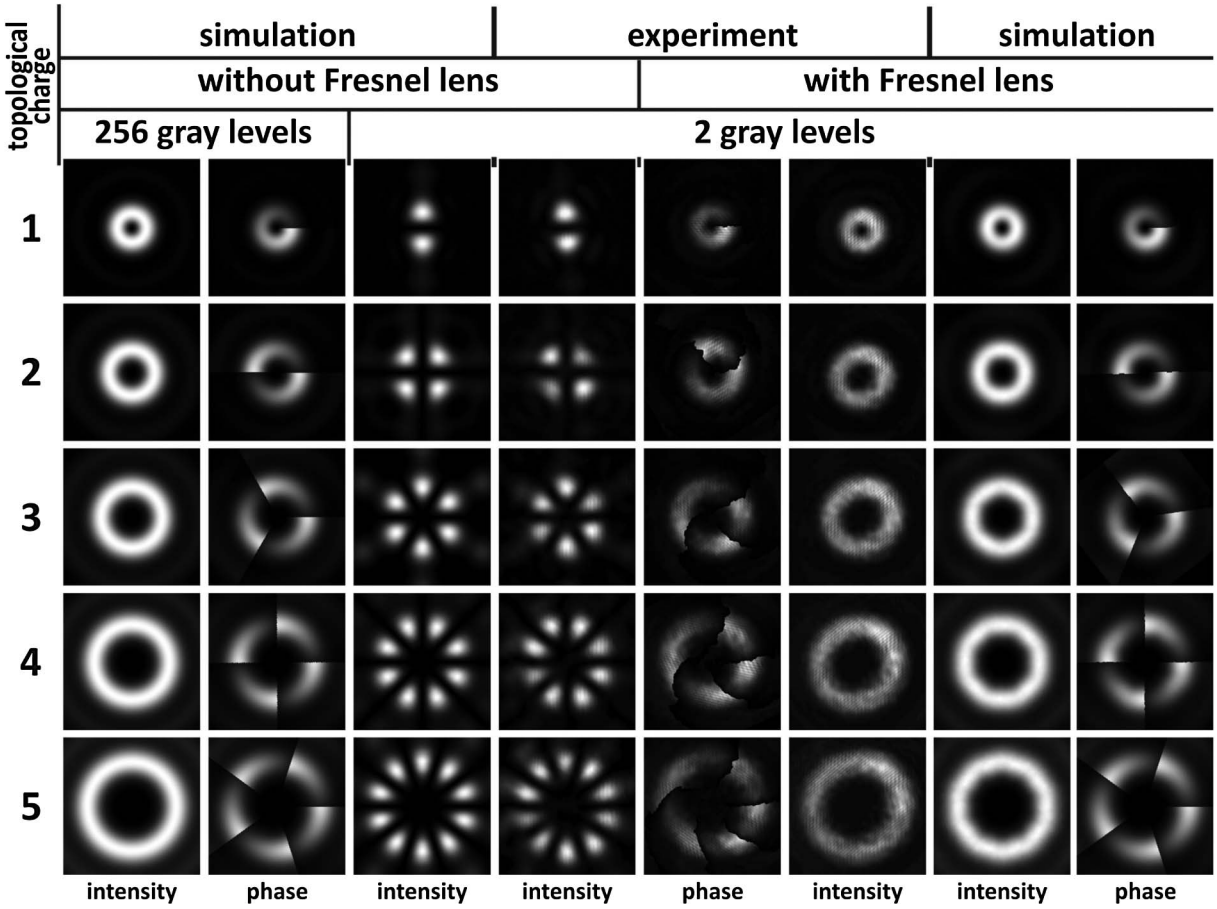

Fig. 4. Laguerre-Gauss-like optical vortices for topological charges $m = 1$ to $m = 5$. With $w = 2.35$ mm, $f_{\mathrm{FR}} = -1.54$ m and $f = 250$ mm. From left to right: intensity and phase simulations of OVs computed with discrete phase masks for $N = 256$; intensity simulations of OVs computed from two-phase level SPPs (without Fresnel lens); intensity of experimental results for two-phase level SPPs and phase and intensity of OVs generated from BVPLs; intensity and phase simulations of OVs computed with BVPL.

obtained computationally with 256 phase levels (ideal vortex), and OVs experimentally reached with only two-phase level VPLs. The normalization was done by using the worst experimental case (I_{wc}):

$$\mathrm{MSE} = \frac{\sum_{i,j} (I_{256}(i,j) - I_2(i,j))^2}{\sum_{i,j} (I_{256}(i,j) - I_{\mathrm{wc}}(i,j))^2}. \tag{1}$$

In Fig. 5 some intensity patterns and their respective MSEs as function of z (for fixed $f_{\mathrm{FR}} \approx -1.54$ m and $w = 2.35$ mm) are presented. In the optimum plane the minimum MSE (close to zero) coincides with the z_{opt}. The intensity patterns of the OVs were registered with steps $\Delta z = 0.5$ mm between each image. The results suggest that the MSE is symmetric with respect to the optimal plane of observation. In this way, for displacements forward and backward to the optimal observation plane, the intensity distributions of the OVs are notably distorted from the ideal case as the distance to z_{opt} increases. This observation confirms the great influence of the observation plane on the quality of the optical vortices generated by using BVPLs. Additionally, it is very important to highlight the high sensibility of the system to small variations of z. In this sense, it is clear that a distance equal to ± 6 mm from the optimal observation plane is enough to distort the vortex intensity distribution,

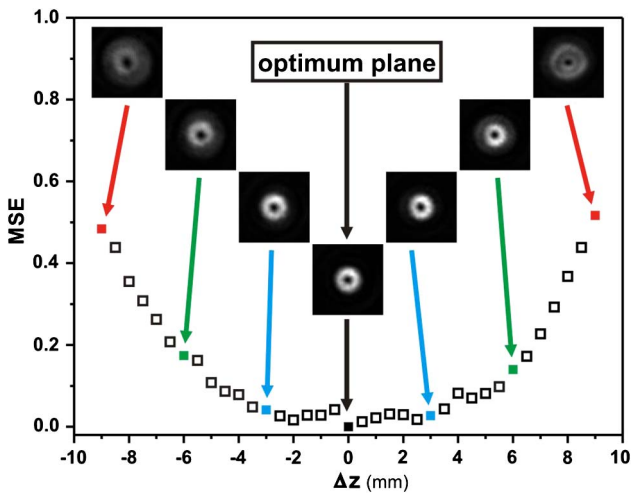

Fig. 5. Quality measurement of the optical vortex (NMSE) around the optimal observation plane. The worst case corresponds to the lack of phase levels (NG = 1) (calculated with $w = 2.35$ mm, $f_{\mathrm{FR}} = -1.54$ m).

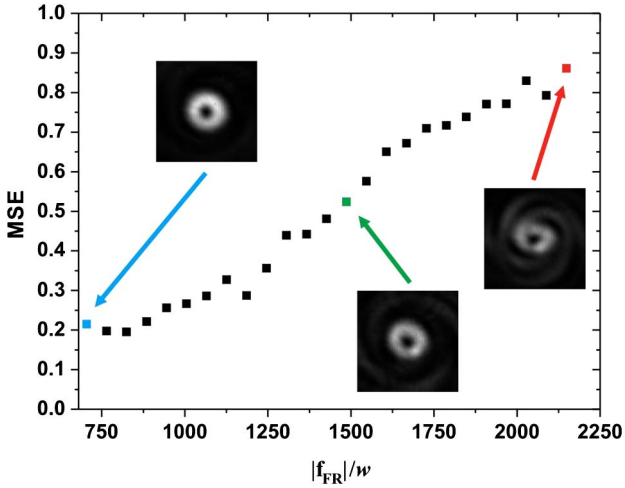

Fig. 6. OV quality dependence as a function of $|f_{FR}|/w$. $w = 2.35$ mm.

and, therefore, there is a strong loss of quality in the OV generated experimentally.

Similarly, in Fig. 6 the dependence of the quality of the OV with the focal length f_{FR} (constant beam radius $w = 2.35$ mm) is presented. In this case, each image was captured by varying the local length in steps of 0.2 m, starting from $f_{FR} \approx -1.54$ m to $f_{FR} \approx -7.14$ m. As the optimal observation plane depends on this parameter, each intensity image was reached after locating the corresponding z position In this case, when the relationship $|f_{FR}|/w$ increases, the MSE rises too, and, therefore, the quality of the vortex decreases. These results can be explained by considering that if the focal length of the Fresnel lens increases, the distance to the observation plane decreases, and z_{opt} decreases accordingly; i.e., after of each step the observation plane is closer to the focal plane of L_2. In turn, this implies that with this condition the BVPL operates as a SPP where the Fresnel lens does not exist, and, as has been presented in Section 2, the two-level SPPs do not create good quality OVs.

4. Conclusions

In this work, the possibility of experimentally generating L-G-like optical vortices by using discrete phase masks of only two levels was demonstrated. As a strategy, a comparison between the experimental results of techniques based on SPPs and BVPLs was developed, and it was demonstrated that the associated BVPLs' performance was much higher than that related to the traditional binary SPPs. By including BVPLs in the experimental setup, it was possible to experimentally generate high-quality OVs of topological charges $m = 1$ to $m = 5$. Those OVs were very similar to those obtained by using SPPs of much more phase levels. Finally, the vortex quality dependency with the focal length of the Fresnel lens and the observation plane was experimentally explored, and the parameters that influenced the performance of the technique were defined. The results of this work open the real possibility of using low-cost spatial light modulators in optical vortices applications.

This research was performed under grants Convocatoria Pública Programática 2012-2013: Área de Ciencias Exactas (Proyecto CODI—256), Proyecto 13129—Convocatoria 2012 Instituto Tecnológico Metropolitano (ITM), and PIP 0549 from CONICET. A. L. thanks Subsidios para viajes y/o Estadías (2013 to 2014) from UNLP and Programa de Becas de Movilidad Académica from AUIP for financial support. E. R. and N. L. thank U de A for financial support. J. A. G. thanks Politécnico Colombiano Jaime Isaza Cadavid.

References

1. J. F. Nye and M. V. Berry, "Dislocations in wave trains," Proc. R. Soc. London Ser. A **336**, 165–190 (1974).
2. M. El Ketara and E. Brasselet, "Observation of self-induced optical vortex precession," Phys. Rev. Lett. **110**, 233603 (2013).
3. J. Leach, M. R. Dennis, J. Courtial, and M. J. Padgett, "Vortex knots in light," New J. Phys. **7**, 55 (2005).
4. R. K. Tyson, M. Scipioni, and J. Viegas, "Generation of an optical vortex with a segmented deformable mirror," Appl. Opt. **47**, 6300–6306 (2008).
5. A. M. Yao and M. J. Padgett, "Orbital angular momentum: origins, behavior and applications," Adv. Opt. Photonics **3**, 161–204 (2011).
6. L. Allen, M. Beijersbergen, R. Spreeuw, and J. Woerdman, "Orbital angular momentum of light and the transformation of Laguerre–Gaussian laser modes," Phys. Rev. A **45**, 8185–8189 (1992).
7. V. Caullet, N. Marsal, D. Wolfersberger, and M. Sciamanna, "Optical patterns using vortex beams," Proc. SPIE **8434**, 84341T (2012).
8. J. E. Curtis, B. A. Koss, and D. G. Grier, "Dynamic holographic optical tweezers," Opt. Commun. **207**, 169–175 (2002).
9. J. E. Curtis and D. G. Grier, "Modulated optical vortices," Opt. Lett. **28**, 872–874 (2003).
10. A. Arias, S. Etcheverry, P. Solano, J. P. Staforelli, M. J. Gallardo, H. Rubinsztein-Dunlop, and C. Saavedra, "Simultaneous rotation, orientation and displacement control of birefringent microparticles in holographic optical tweezers," Opt. Express **21**, 102–111 (2013).
11. S. Fürhapter, A. Jesacher, S. Bernet, and M. Ritsch-Marte, "Spiral phase contrast imaging in microscopy," Opt. Express **13**, 689–694 (2005).
12. J. A. Gómez, E. Rueda, Á. Salazar, M. Tebaldi, N. Bolognini, and A. Lencina, "Effects of the induced birefringence in photorefractive crystals on speckle optical vortices," Opt. Eng. **50**, 359–365 (2012).
13. J. A. Davis, D. E. McNamara, D. M. Cottrell, and J. Campos, "Image processing with the radial Hilbert transform: theory and experiments," Opt. Lett. **25**, 99–101 (2000).
14. K. Crabtree, J. A. Davis, and I. Moreno, "Optical processing with vortex-producing lenses," Appl. Opt. **43**, 1360–1367 (2004).
15. A. Mair, A. Vaziri, G. Weihs, and A. Zeilinger, "Entanglement of orbital angular momentum states of photons," Nature **412**, 313–316 (2001).
16. G. Gibson, J. Courtial, and M. J. Padgett, "Free-space information transfer using light beams carrying orbital angular momentum," Opt. Express **12**, 5448–5456 (2004).
17. J. H. Lee, G. Foo, E. G. Johnson, and G. A. Swartzlander, Jr., "Experimental verification of an optical vortex coronagraph," Phys. Rev. Lett. **97**, 0539011 (2006).
18. M. Padgett, J. Courtial, and L. Allen, "Light's orbital angular momentum," Phys. Today **57**(5), 35–40 (2004).
19. Q. Wang, X. W. Sun, and P. Shum, "Dynamic switching of optical vortices with dynamic gamma-correction liquid crystal spiral phase plate," Opt. Express **13**, 10285–10291 (2005).

20. E. Rueda, D. Muñetón, J. A. Gómez, and A. Lencina, "High-quality optical vortex-beam generation by using a multilevel vortex-producing lens," Opt. Lett. **38**, 3941–3944 (2013).
21. C. S. Guo, D. M. Xue, Y. J. Han, and J. Ding, "Optimal phase steps of multi-level spiral phase plates," Opt. Commun. **268**, 235–239 (2006).
22. V. V. Kotlyar and A. A. Kovalev, "Fraunhofer diffraction of the plane wave by a multilevel (quantized) spiral phase plate," Opt. Lett. **33**, 189–191 (2008).
23. N. Zhang, J. A. Davis, I. Moreno, D. M. Cottrell, and X.-C. Yuan, "Analysis of multilevel spiral phase plates using a Dammann vortex sensing grating," Opt. Express **18**, 25987–25992 (2010).
24. C. S. Guo, Z. Y. Rong, H. T. Wang, Y. Wang, and L. Z. Cai, "Phase-shifting with computer-generated holograms written on a spatial light modulator," Appl. Opt. **42**, 6975–6979 (2003).
25. E. Hecht, *Optics*, 4th ed. (Addison-Wesley, 2002), p. 246.
26. A. Y. Bekshaev, M. S. Soskin, and M. V. Vasnetsov, "Transformation of higher-order optical vortices upon focusing by an astigmatic lens," Opt. Commun. **241**, 237–247 (2004).